Proximity Effects in Self-Organized Binary Particle–Block Copolymer Blends

Michael R. Bockstaller* and Edwin L. Thomas

Massachusetts Institute of Technology, Center of Materials Science and Engineering and Institute of Soldier Nanotechnologies, 77 Massachusetts Avenue, Cambridge, 02139 Massachusetts, USA

(Received 2 March 2004; published 15 October 2004)

Dependent on the surface chemistry of gold nanocrystals of equal metal core size, two morphological types of self-organized block copolymer–particle blends are observed: (1) the segregation of the nanocrystals to the interfacial areas or (2) the preferential uniform distribution within one of the respective polymer domains. The confinement of the nanocrystals to the narrow interfacial regions of the microstructure in type one blends results in high local particle filling fractions and gives rise to electromagnetic coupling upon light irradiation, accompanied by a pronounced increase in absorbance.

DOI: 10.1103/PhysRevLett.93.166106 PACS numbers: 81.07.-b, 81.05.Qk, 81.16.Dn, 82.35.Np

The template-driven organization of nanoscopic matter provides opportunities for novel high-performance materials that capitalize on the synergism between the physical properties of the matrix and the unique properties of nanosized matter [1,2].

In this contribution we demonstrate the influence of particle distribution within binary block copolymer/metal nanocrystal mixtures on the resultant optical properties of the composite. The material system in our study consists of a selective host matrix comprised of near-symmetric poly(styrene-*b*-ethylene propylene) copolymer (PS_{3600}-PEP_{6500}, indices denote the degree of polymerization) and dodecyl and oligo(styrene) (nine monomer units) coated gold nanocrystals with a mean metal core diameter of $2R = 3$ and 3.5 nm, respectively [3]. The lamellar morphology of the block copolymer with domain spacing of $L_{PS} = 100$ nm for the PS and $L_{PEP} = 80$ nm for the PEP domain was confirmed by ultrasmall angle x-ray scattering and transmission electron microscopy, respectively. Electron micrographs obtained after sectioning the films *normal* to the layer direction as shown in Fig. 1, reveal two distinct types of particle arrangements within the composite dependent on the particle's surface functionality. Dodecyl coated nanocrystals are localized exclusively at the intermaterial dividing surface (IMDS) separating the polymer microdomains resulting in thin, layerlike particle assemblies. In contrast, oligo(styrene) coated nanocrystals preferentially but uniformly sequester within the PS domain of the PS-PEP block copolymer with a selectivity ratio of $N_{Au}(PS)/N_{Au}(PEP) \approx 8.5$, with $N_{Au}(X)$ denoting the respective number of gold nanocrystals within domain X. These findings are unexpected since recent theoretical studies suggest that the competition between the particle's translational entropy and the chain configurational entropy should result in the interfacial segregation of the nanocrystals within the composite in the limit of $R \ll L_X$ and in domain-center alignment of the particles in the limit of $R/L_X \approx 1$, with L_X denoting the thickness of the particle host domain [4]. The contour length of the surface grafted ligands can be estimated to be $l_{aliph} \cong 0.9$ nm and $l_{PS} \cong 1.8$ nm for dodecyl and oligo(styrene) ligands, resulting in a particle-to-polymer domain size ratio of $(R + l_{lig})/(L_{PS} + L_{PEP}) = 0.045$ for the PS and 0.024 for the aliphatic coated nanocrystals. We thus reason that a difference in enthalpic compatibilization that was not accounted for previously to be the main origin of the different particle distributions.

In the present Letter we focus on the effect of the particle proximity within the microstructure on the resulting optical properties. For convenience, we abbreviate the two different particle distributions as type I, denoting the interfacial segregated type (representing the PS-PEP/$AuSC_{12}H_{25}$ composition), and type U, denoting the selective-layer uniformly dispersed case (representing the PS-PEP/AuSPS composition). The optical properties of type I and U films were characterized using a Cary 5E UV-vis-NIR dual-beam spectrophotometer equipped with a polarizer and a diffuse reflectance accessory facilitating the concurrent determination of the sample's reflectivity and transmittance. For specimens with equal film thickness ($t \approx 100$ μm), the sample's absorptance Λ was obtained by $\Lambda = (I_0 - I_T - I_R)/I_0$ with I_T/I_0 and I_R/I_0 denoting the sample's transmittance and reflectance, respectively. Shown in Fig. 2 are the absorptance spectra that were obtained for type I and U films revealing a significant increase in absorption losses as well as a redshift and broadening of the absorption peak in the case of the type I sample. Note that the respective particle volume filling fractions of the two nanocomposites are practically equal ($\phi_{AuSPS} = 0.01$ and $\phi_{AuSC12H25} = 0.013$, as determined by elemental analysis). The difference in the optical response of the two composite morphologies becomes more intriguing as the optical properties of the respective ligand coated neat nanocrystal samples are found to be practically identical as demonstrated in the absorption spectra of the dodecyl and PS coated nanocrystals in toluene solution shown in the inset of Fig. 2.

A qualitative understanding of the observed phenomena can be obtained by considering the different local particle environments that are imposed by the

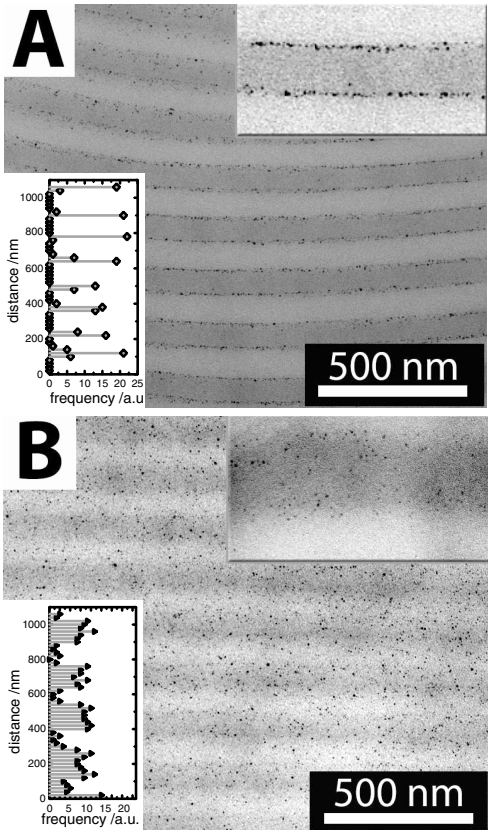

FIG. 1. Bright field transmission electron micrographs of the unstained block copolymer/nanocrystal composite material after microsectioning *normal* to the layer direction demonstrating particle deposition at the IMDS (PS-PEP/$AuSC_{12}H_{25}$, type I) in panel A and homogeneous selective-layer morphology (PS-PEP/AuSPS, type *U*) in panel B, respectively. PEP domains appear as brighter regions in the micrograph. The volume filling fraction of gold for both samples is $\phi \approx 0.01$. The lower insets in panel A and B depict the respective particle frequencies in 00l direction obtained by particle counting in equally sized area elements of 20 nm width. In panel B, a small amount of tilt of the IMDS with respect to the electron beam direction results in a somewhat smeared appearance of the PS-PEP interface.

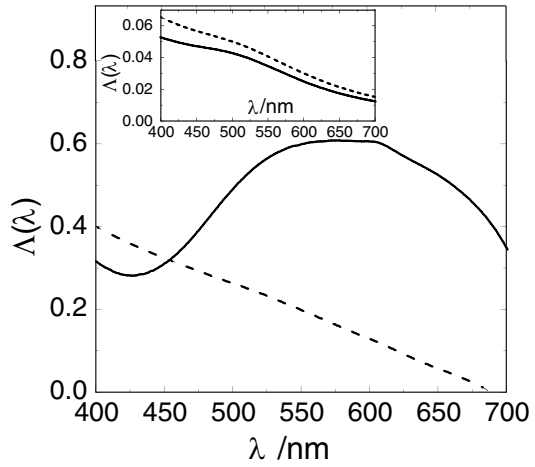

FIG. 2. Absorptance spectra of block copolymer/nanocrystal composite materials with interfacial segregated morphology (dotted line) as well as selective-layer uniform morphology (continuous line). Inset: absorptance spectra of dilute nanocrystal solutions (concentration $c = 0.001\%$ (w/v) in toluene) representing $AuSC_{12}H_{25}$ (dotted line) and AuSPS (continuous line), respectively.

self-assembled domain microstructure. Figure 3 shows an electron micrograph obtained after microsectioning the type I sample *parallel* to the layer orientation. The thickness of the section (~50 nm) is thinner than the lamellar period allowing the lateral distribution of nanocrystals along an individual IMDS to be determined. Note that despite the overall low metal filling fraction, layers with dense particle coverage form in between the polymer domains due to the spatial confinement of the nanocrystals to the narrow interfacial regions. The pair distribution function $g(r)$ calculated from the particle positions along the interface shown in the inset of Fig. 3 indicates that the particle assemblage is not due to a diffusion limited aggregation mechanism for which $g(r) \propto 1/r^{2-D}$ (with D the fractal mass parameter) would be expected and suggests a rather isotropic particle interaction not significantly exceeding thermal energy [5]. The average minimum distance between neighboring particles is larger than the particle core diameter, i.e., $\langle r \rangle \approx 1.25\ (2R)$, indicating a somewhat stretched conformation of the aliphatic surfactant groups that act as impenetrable shells around the particle cores and increase the effective par-

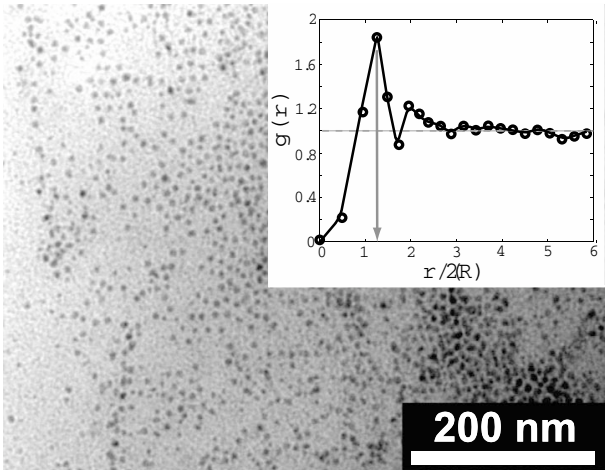

FIG. 3. Bright field electron micrograph of the unstained block copolymer/$AuSC_{12}H_{25}$ (interfacial segregated morphology) composite material after sectioning *parallel* to the layer direction revealing the particle distribution along an individual dividing surface. The total gold volume filling fraction is $\phi \approx 0.01$. The image analysis was performed using the free software package SCION IMAGE [11]. Gold nanocrystals appear randomly dispersed along the IMDS with an area coverage of $\phi_I \approx 0.23 \pm 0.02$. Inset: Calculated pair distribution function $g(\mathbf{r}) = \langle N/a \rangle^{-1} dN(\mathbf{r}, \mathbf{r} + d\mathbf{r})/da(\mathbf{r}, \mathbf{r} + d\mathbf{r})$, with $\langle \ldots \rangle$ denoting the ensemble average, $\mathbf{r}$ is the distance vector, and N the number of particles located in the area a.

ticle size. Given a total metal volume filling fraction of $\phi = 0.01$ and assuming the thickness of an interfacial layer to be 3 nm (equal to the particle diameter) the average particle filling fraction within an interfacial layer can be estimated to be $\phi_I \approx 0.3$. This is in reasonable agreement to experimental values that can be obtained from electron micrographs like the one shown in Fig. 3 where the average volume filling fraction of the metal component in the interfacial region can be determined from the particle area coverage to be $\phi_I = 0.23 \pm 0.05$. The increase in local particle filling fraction along the particle containing IMDS is accompanied by a pronounced decrease between the mean nearest neighbor particle distances $\langle r \rangle$ that can be estimated from the peak position in $g(r)$ to be $\langle r_I \rangle \approx 4$ nm for particles confined within the interfacial regions and $\langle r_U \rangle \propto \langle r_I \rangle^{2/3} L_{\mathrm{PS}}{}^{1/3} \approx 12$ nm for particles that are uniformly dispersed within the PS layers.

The increase and the redshift in absorption that is observed in case of the interfacial segregated particle morphology can be understood by considering the dipolar coupling of plasmon excitation modes that occur in closely spaced metal nanocrystal assemblies [6]. As a simplified model system that qualitatively displays the phenomena of proximity effects, we consider here an ensemble of crystal pairs located within a plane (representing the IMDS) with an orientation towards the incident electric field defined by $\theta = \angle(\mathbf{E}, \mathbf{r})$, where $\mathbf{E}$ denotes the electric field vector of the linearly polarized light and $\mathbf{r}$ the particle-particle distance vector as indicated in Fig. 4(a). θ can be expressed as $\theta = \arccos(\cos\beta \cos\gamma)$ where β is the orientation angle of the crystal pair within the plane and γ accounts for the partial tilting of the polymer layers with respect to the incident beam due to defect formation within the microstructure. For a 2D isotropic distribution of the nanocrystals within the plane, β is randomly distributed within the interval $[0, 2\pi]$, whereas γ has to be determined from large-area electron micrographs of sectioned films. The maximum deviation of the layer orientation from normal incidence for specimen areas of 1 mm^2 (corresponding to the typical areas tested in the optical experiments) was found to be $\gamma_{\max} \approx 20^\circ = \pi/9$. We thus assume that γ can be represented by a standard normal distribution $P(\gamma) = 18/(\pi\sqrt{2\pi}) \exp[-162\gamma^2/\pi^2]$. Since the particle diameter $2R$ as well as the particle center-to-center distance r are much smaller than the wavelength of the incident light (quasistatic approximation), we can write the normalized polarizability of the crystal pair parallel to the incident field

$$\Pi_{\mathrm{pair}} = \alpha \int \left(\frac{\sin^2\theta}{1 + C\alpha/r^3} + \frac{\cos^2\theta}{1 - 2C\alpha/r^3} \right) W(\theta) d\theta \Big/ \int W(\theta) d\theta, \quad (1)$$

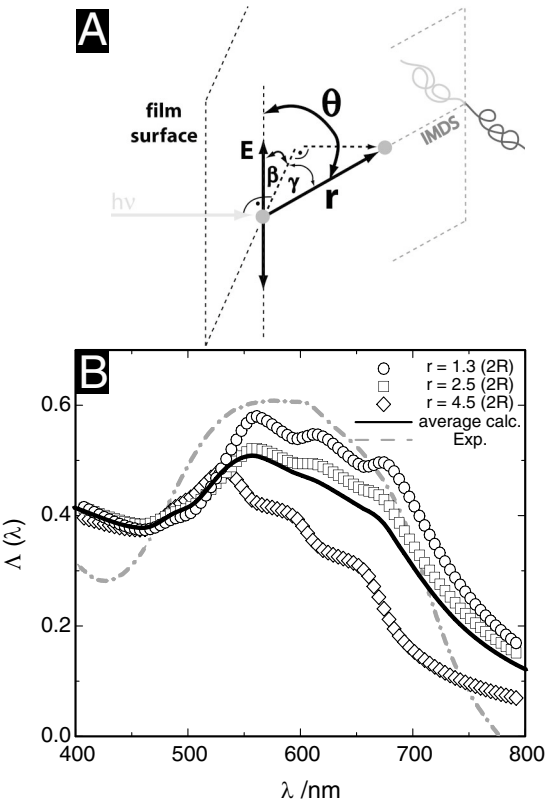

FIG. 4. Panel A. Schematic of the particle arrangement. Panel B. Calculated absorptance spectra for a stack of gold nanocrystal pair containing interfaces (representing the crystal pairs located along the IMDS) assuming 10^3 layers, a particle area density of $3 \times 10^{12}/\mathrm{cm}^2$, a particle diameter $2R = 3$ nm, and a center-to-center distance $r = 1.3(2R)$ ○ and $r = 2.5(2R)$ □ using the electrostatic approximation Eq. (1) for a distribution of layer orientations similar to the block copolymer materials (for details see text). ◇ represents the absorptance of an individual nanocrystal [equal to $r = 4.5(2R)$]. The black continuous line is the average absorptance spectra calculated assuming equal proportion of the different crystal arrangements and the dash-dotted line is the experimental absorptance spectrum. The optical constants of the gold nanocrystals were determined according to Palik [10] the matrix dielectric function is $\varepsilon_{\mathrm{PS}} = 2.53$.

with the single particle polarizability given by $\alpha = 4\pi\varepsilon_0 R^3[\varepsilon_p(\omega) - \varepsilon_m]/[\varepsilon_p(\omega) + 2\varepsilon_m]$, and $C = (4\pi\varepsilon_0\varepsilon_m)^{-1}$, where ε_0 is the permittivity of free space and $\varepsilon_p(\omega)$ and $\varepsilon_m = 2.53$ denote the frequency dependent crystal and matrix dielectric function, respectively [7]. $W(\theta)$ is a weighting function that takes into account the tilting of the layers about the normal and is determined numerically.

As discussed by several authors, the short-ranged electrostatic interactions that result from the dipolar coupling between neighboring nanocrystals are weighted by r^{-3} and therefore are relevant only in closely spaced particle array structures [8]. The crystal-pair absorption cross section can be calculated following the

Lorentz-Lorenz relation as $C^{\mathrm{abs}}(\omega) = (\omega/c)\mathrm{Im}\{\varepsilon_m(1 + 2C'\phi_I\Pi_{\mathrm{pair}})(1 - C'\phi_I\Pi_{\mathrm{pair}})^{-1}\}$, with c denoting the vacuum velocity of light, $C' = CR^{-3}$ and $\mathrm{Im}\{Y\}$ the imaginary part of Y, as a function of the particle center-to-center distance assuming a crystal diameter of $2R = 3$ nm [9,10]. The sample's absorptance is then related to the absorption cross section via $\Lambda = 1 - \exp[-ntC^{\mathrm{abs}}]$, where t denotes the sample thickness and n the particle number density. Figure 4(b) depicts the calculated absorptance spectra after numerical evaluation of Eq. (1) for a set of 10^3 crystal pairs assuming a particle number density of $n = 3 \times 10^{12}$ particles/cm^2 (equal to $\phi_I \approx 0.2$) along each interface and a sample thickness of $t = 100$ μm, corresponding to about 10^3 interfaces stacked normal to the propagation direction of the incoming light. Clearly, decreasing the particle distance is predicted to redshift the plasmon resonance of the crystal pair as well as to result in a pronounced broadening of the absorption spectra. For particle distances between $r = 2.4R$ and $r = 4.5R$ the wavelength of maximum absorption is expected to be shifted within the spectral range $550 \leq \lambda \leq 750$ nm. The resulting average optical response of the nanocrystal-pair arrangements shows qualitative agreement with our experimental data. At larger particle distances the coupling effects vanish and the absorptance of the pair approaches that of two isolated particles.

The enhanced absorption that is observed in the case of the interfacial segregated composite morphology demonstrates that the optical properties of microstructured heterogeneous materials sensibly depend on the interrelationship between nanosize specific material characteristics and the local environment imposed by the morphology of the material. These findings underline the importance of structural control in multicomponent materials for optimizing the materials performance and for the utilization of synergistic effects. We note that the approach of tailored particle location should be equally well applicable to 2D cylindrical and 3D cubic discrete spherical or bicontinuous network (i.e., double gyroid) morphologies that will be the subject of future studies.

This research was supported in part by the U.S. Army through the Institute for Soldier Nanotechnologies, under Contract No. DAAD-19-02-D0002 with the U.S. Army Research Office as well as the Alexander von Humboldt Foundation (Feodor-Lynen program).

*Author to whom correspondence should be addressed.
Electronic address: Bockstaller@dwi.rwth-aachen.de, elt@mit.edu
Present address: Institute for Technical and Macromolecular Chemistry, RWTH Aachen, Worringerweg 1, D-52074 Aachen, Germany.

[1] M. R. Bockstaller, R. Kolb, and E. L. Thomas, Adv. Mater. **13**, 1783 (2001); C. Park, J. Yoon, and E. L. Thomas, Polymer **44**, 6725 (2003).
[2] Y. A. Vlasov and D. J. Norris, Adv. Mater. **13**, 371 (2001).
[3] See EPAPS Document No. E-PRLTAO-93-061441 for details on synthesis and sample preparation. A direct link to this document may be found in the online article's HTML reference section. The document may also be reached via the EPAPS homepage (http://www.aip.org/pubservs/epaps.html) or from ftp.aip.org in the directory /epaps/. See the EPAPS homepage for more information. See also: M. R. Bockstaller, and E. L. Thomas, J. Phys. Chem. B **107**, 10017 (2003); M. R. Bockstaller, Y. Lapetnikov, S. Margel, and E. L. Thomas, J. Am. Chem. Soc. **125**, 5276 (2003).
[4] J. Huh, V. V. Ginzburg, and A. C. Balazs, Macromolecules **33**, 8085 (2000); R. B. Thompson, V. V. Ginzburg, M. W. Matsen, and A. C. Balazs, Science **292**, 2469 (2001).
[5] T. A. Witten and L. M. Sanders, Phys. Rev. Lett. **47**, 1400 (1981).
[6] W. Trinks, Ann. Phys. (Leipzig) **22**, 561 (1935); M. Quinten, A. Leitner, J. R. Krenn, and F. R. Aussenegg, Opt. Lett. **23**, 1331 (1998).
[7] M. Quinten, U. Kreibig, and D. Schonauer, Surf. Sci. **156**, 741 (1985).
[8] L. Zhao, K. L. Kelly, and C. G. Schatz, J. Phys. Chem. B **107**, 7343 (2003); B. Lamprecht *et al.*, Phys. Rev. Lett. **84**, 4721 (2000); L. C. Haynes *et al.*, J. Phys. Chem. B **107**, 7337 (2003).
[9] M. Born and M. Wolf, *Theory of Optics* (Cambridge University Press, London, 2000).
[10] Optical constants were taken from Palik [see E. D. Palik, *Handbook of Optical Constants of Solids* (Academic Press, San Diego, 1998), Vol. 1]. Size corrections to the particle dielectric function were taken into account following Fragstein *et al.* [see U. Fragstein and U. Kreibig, Z. Phys. **224**, 307 (1969)].
[11] Available at http://www.scioncorp.com/